Numer. Math. Theor. Meth. Appl.
doi: 10.4208/nmtma.2015.w07si

Vol. **8**, No. 1, pp. 78-96
February 2015

Local Fourier Analysis for Edge-Based Discretizations on Triangular Grids

Carmen Rodrigo[1,*], Francisco Sanz[2], Francisco J. Gaspar[3] and Francisco J. Lisbona[3]

[1] *Department of Applied Mathematics, University of Zaragoza, C/ Maria de Luna 3, 50018, Zaragoza, Spain.*
[2] *BIFI University of Zaragoza, C/ Pedro Cerbuna 12, 50009, Zaragoza, Spain.*
[3] *Department of Applied Mathematics, University of Zaragoza, C/ Pedro Cerbuna 12, 50009, Zaragoza, Spain.*

Received 2 November 2013; Accepted 22 June 2014

Abstract. In this paper, we present a local Fourier analysis framework for analyzing the different components within multigrid solvers for edge-based discretizations on triangular grids. The different stencils associated with edges of different orientation in a triangular mesh make this analysis special. The resulting tool is demonstrated for the vector Laplace problem discretized by mimetic finite difference schemes. Results from the local Fourier analysis, as well as experimentally obtained results, are presented to validate the proposed analysis.

AMS subject classifications: 65F10, 65N22, 65N55

Key words: Multigrid, local Fourier analysis, edge-based discretizations, mimetic finite differences.

1. Introduction

In the numerical simulation of problems modeled by partial differential equations, the linear system solvers play a key role. Efficient algorithms enable large-scale computations with a satisfactory computing time and memory consumption. As is well-known, multigrid methods are among the most powerful techniques for this purpose. Since the 70's, when these methods [5,9,15,18] were developed, they have become very popular within the scientific community. Many approaches to multigrid theory have been investigated in the last years; among these, the technique of local Fourier analysis (LFA), introduced by Brandt [5,6], has become very successful, providing accurate predictions of performance for a variety of problems.

*Corresponding author. *Email addresses:* carmenr@unizar.es (C. Rodrigo), frasanz@bifi.es (F. Sanz), fjgaspar@unizar.es (F. J. Gaspar), lisbona@unizar.es (F. J. Lisbona)

LFA does not only provide accurate asymptotic convergence rates of the algorithms, but also is a useful technique for choosing suitable components for multigrid methods. Wienands and Joppich [19] provide a useful software tool for experimenting with Fourier analysis. Recent advances in this context include LFA for multigrid as a preconditioner [20], for triangular meshes [7, 14], optimal control problems [3], and discontinuous Galerkin discretizations [8]. In this paper, we present a framework for performing the local Fourier analysis for edge based discretizations on triangular grids. Although for simplicity in the presentation, we restrict ourselves to the two-dimensional case, we would like to emphasize that the technique presented here is easily extended to the three-dimensional case.

Mainly as a result of its good computational properties, edge-based discretizations have emerged widely in the simulation of many real applications, including electromagnetic field computations. Examples of such discretizations include Nédélec and Raviart-Thomas finite element methods and mimetic finite difference schemes. While in standard nodal discretizations, the unknowns are located at the nodes of a target grid, in case of edge-based schemes, the unknowns are associated with the edges of the corresponding mesh. Moreover, different stencils are associated with edges of different orientation. It is obvious that existing schemes for multigrid solution on nodal discretizations can not be used directly for edge-based schemes. Therefore, some efforts to implement multigrid solution schemes for edge based discretizations have been carried out recently, see for example [1, 2, 10, 11, 13]. For edge-based discretizations on triangular meshes, quantitative estimates of the multigrid methods as a function of the components chosen are missing in the literature. This question is at the focus of this paper.

Our aim is therefore to present a tool based on Fourier analysis, which does not only provide accurate asymptotic convergence rates, but also gives advice for an adequate composition of methods. To carry out this analysis in the framework of edge-based discretizations, several particular aspects have to be taken into account. First, the basis of LFA on triangular grids has to be considered, and also we have to deal with a discrete operator which is defined in a different way depending on the orientation of the edges, as we will see. To illustrate this analysis, mimetic finite difference schemes will be considered as example. This discretization is based on the discrete analogies of first-order differential operators, div, **grad**, rot and **curl**, that satisfy discrete analogies of the theorems of vector analysis, see for example [16]. Notice that other approaches e.g., the electromagnetic FIT [17] or Whitney element methods [4], have also been recognized as mimetic discretizations, see [12] for a review of all these techniques.

The remainder of the paper is organized as follows. In Section 2, a framework for the local Fourier analysis for general edge-based discretizations is developed. Section 3 introduces the mimetic finite difference scheme considered here to show the suitability of the presented analysis. To this purpose, in Section 4 some results of LFA for this type of discretization for a vector model problem, more concretely for the vector Laplace operator, are presented. Finally, in Section 5 some conclusions are drawn.

2. Local Fourier analysis for edge-based discretizations

Although for simplicity in the presentation we only consider discretizations having one unknown per edge, this analysis can be easily extended to discretizations having several unknowns per edge (high-order discretizations). Local Fourier analysis is based on the Discrete Fourier Transform, and some reasonable assumptions have to be done to perform this analysis; an infinite regular grid is considered, where formally the discrete operator is represented by a constant discretization stencil, and boundary conditions are not taken into account.

The application of this analysis to edge-based discretizations is not straightforward. First of all, the ideas about the recently introduced LFA on triangular grids [7, 14] have to be taken into account. The key fact for this extension is to consider an expression of the Fourier transform in new coordinate systems in space and frequency variables. To this purpose, we establish a non-orthogonal unit basis of $\mathbb{R}^2$, $\{\mathbf{e}_1, \mathbf{e}_2\}$, which is chosen fitting the geometry of the given mesh, as seen in Fig. 1 (a), and the basis corresponding to the frequencies space, $\{\mathbf{e}'_1, \mathbf{e}'_2\}$, is taken as its reciprocal basis, see Fig. 1 (b); that is, the vectors of the bases satisfy $(\mathbf{e}_i, \mathbf{e}'_j) = \delta_{ij}$, $1 \leq i, j \leq 2$.

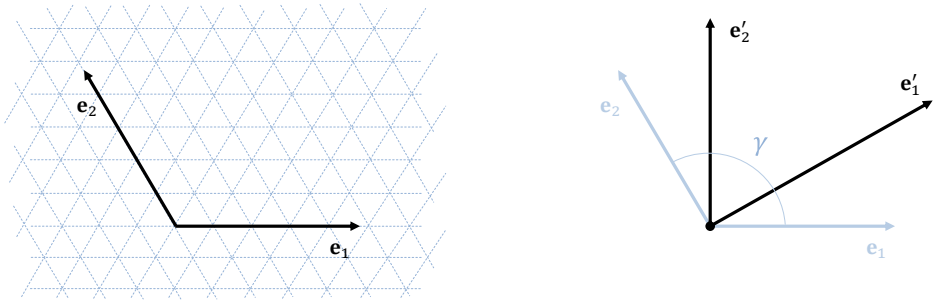

(a) (b)

Figure 1: (a) $\{\mathbf{e}_1, \mathbf{e}_2\}$ non-orthogonal basis on $\mathbb{R}^2$, and (b) reciprocal bases $\{\mathbf{e}_1, \mathbf{e}_2\}$ and $\{\mathbf{e}'_1, \mathbf{e}'_2\}$.

Furthermore, the notion of staggered grids for discretizations of systems of partial differential equations on rectangular grids has to be extended to edge-based discretizations on triangular grids. In this type of discretizations, there are unknowns located at different types of grid-points, and therefore the stencils defining the discrete operator on each point-type involve different surrounding unknowns, hence the discrete operator is not defined in the same way at all grid-points. This fact has to be considered in the analysis for this type of discretizations.

First of all, as an infinite grid has to be considered, the original grid is extended to the following infinite grid $G_h = \bigcup_{j=1}^{3} G_h^j$, see Fig. 2 (a), given as the union of three different subgrids

$$G_h^j := \{\mathbf{x}_{k_1,k_2}^j = ((k_1 + \delta_1^j)\, h_1\, \mathbf{e}_1, (k_2 + \delta_2^j)\, h_2\, \mathbf{e}_2) \,|\, k_1, k_2 \in \mathbb{Z}\}, \tag{2.1}$$

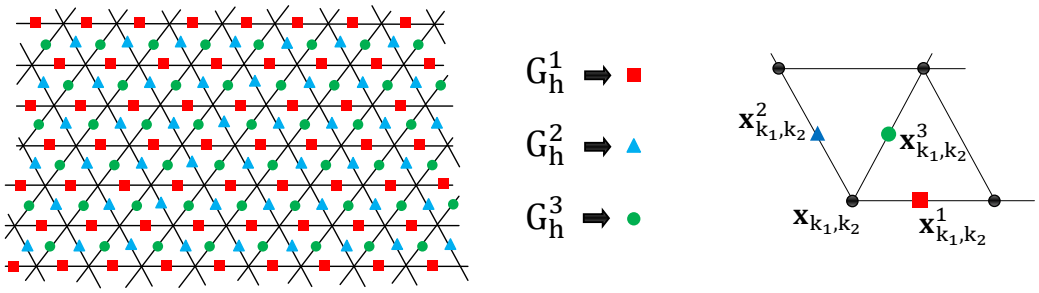

(a) (b)

Figure 2: (a) Infinite grid, composed of three different infinite subgrids. (b) Location of the different unknowns, and correspondence to the three different subgrids, together with the local numbering for the grid-points.

where

$$(\delta_1^j, \delta_2^j) = \begin{cases} (1/2, 0), & \text{if } j = 1, \\ (0, 1/2), & \text{if } j = 2, \\ (1/2, 1/2), & \text{if } j = 3. \end{cases} \tag{2.2}$$

Notice that each of these subgrids G_h^j is associated with a type of edge, that is, to each one of the three different orientations, as we can see in Fig. 2 (b). In order to extend the definition of the discrete operator to the infinite grid G_h, we have to take into account that the resulting equations at grid-points on G_h^1, G_h^2 and G_h^3 are different. Thus, we can define the application of the discrete operator to a grid function u_h on G_h in the following way:

$$\begin{aligned} L_h\, u_h(\mathbf{x}) &= \begin{cases} L_h^{11} u_h(\mathbf{x}^1_{k_1,k_2}) + L_h^{12} u_h(\mathbf{x}^2_{k_1,k_2}) + L_h^{13} u_h(\mathbf{x}^3_{k_1,k_2}), & \mathbf{x} = \mathbf{x}^1_{k_1,k_2} \in G_h^1 \\ L_h^{21} u_h(\mathbf{x}^1_{k_1,k_2}) + L_h^{22} u_h(\mathbf{x}^2_{k_1,k_2}) + L_h^{23} u_h(\mathbf{x}^3_{k_1,k_2}), & \mathbf{x} = \mathbf{x}^2_{k_1,k_2} \in G_h^2 \\ L_h^{31} u_h(\mathbf{x}^1_{k_1,k_2}) + L_h^{32} u_h(\mathbf{x}^2_{k_1,k_2}) + L_h^{33} u_h(\mathbf{x}^3_{k_1,k_2}), & \mathbf{x} = \mathbf{x}^3_{k_1,k_2} \in G_h^3 \end{cases} \\ &= \begin{cases} \displaystyle\sum_{l=1}^{3} \Big(\sum_{(i,j)\in I^{1l}} s_{i,j}^{1l} u_h(\mathbf{x}^l_{k_1+i,k_2+j}) \Big), & \mathbf{x} = \mathbf{x}^1_{k_1,k_2} \in G_h^1, \\ \displaystyle\sum_{l=1}^{3} \Big(\sum_{(i,j)\in I^{2l}} s_{i,j}^{2l} u_h(\mathbf{x}^l_{k_1+i,k_2+j}) \Big), & \mathbf{x} = \mathbf{x}^2_{k_1,k_2} \in G_h^2, \\ \displaystyle\sum_{l=1}^{3} \Big(\sum_{(i,j)\in I^{3l}} s_{i,j}^{3l} u_h(\mathbf{x}^l_{k_1+i,k_2+j}) \Big), & \mathbf{x} = \mathbf{x}^3_{k_1,k_2} \in G_h^3, \end{cases} \end{aligned} \tag{2.3}$$

where values $s_{i,j}^{kl}$ are the coefficients corresponding to the stencil of discrete operator L_h^{kl} which gives the relation that exists in the corresponding equation between one unknown in G_h^k and the unknowns in G_h^l. Subsets I^{kl} give the connections of a grid-point located at G_h^k with those in G_h^l. In order to illustrate the definition of the discrete operator, we consider the lowest order Nédélec finite element discretization of operator

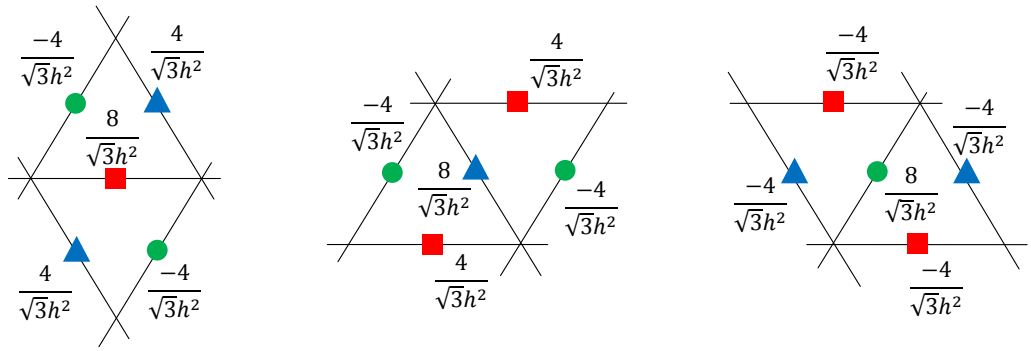

Figure 3: Stencils for operator $\mathbf{curl}\,\mathrm{rot}$ obtained by the lowest order Nédélec FEM for equilateral triangular grids, corresponding to grid-points located at (a) G_h^1, (b) G_h^2, and (c) G_h^3.

$\mathbf{curl}\,\mathrm{rot}$ on equilateral triangular grids. The obtained stencils for the three different grid-points are given in Fig. 3. However, we can write these stencils with the notation previously given in the following way:

$$L_h^{11} = \tfrac{8}{\sqrt{3}h^2}\begin{bmatrix} 0 & 0 & 0 \\ 0 & 1 & 0 \\ 0 & 0 & 0 \end{bmatrix}, \quad L_h^{12} = \tfrac{4}{\sqrt{3}h^2}\begin{bmatrix} 0 & 0 & 0 \\ 0 & 0 & 1 \\ 0 & 1 & 0 \end{bmatrix}, \quad L_h^{13} = \tfrac{-4}{\sqrt{3}h^2}\begin{bmatrix} 0 & 0 & 0 \\ 0 & 1 & 0 \\ 0 & 1 & 0 \end{bmatrix},$$

$$L_h^{21} = \tfrac{4}{\sqrt{3}h^2}\begin{bmatrix} 0 & 1 & 0 \\ 1 & 0 & 0 \\ 0 & 0 & 0 \end{bmatrix}, \quad L_h^{22} = \tfrac{8}{\sqrt{3}h^2}\begin{bmatrix} 0 & 0 & 0 \\ 0 & 1 & 0 \\ 0 & 0 & 0 \end{bmatrix}, \quad L_h^{23} = \tfrac{-4}{\sqrt{3}h^2}\begin{bmatrix} 0 & 0 & 0 \\ 1 & 1 & 0 \\ 0 & 0 & 0 \end{bmatrix},$$

$$L_h^{31} = \tfrac{-4}{\sqrt{3}h^2}\begin{bmatrix} 0 & 1 & 0 \\ 0 & 1 & 0 \\ 0 & 0 & 0 \end{bmatrix}, \quad L_h^{32} = \tfrac{-4}{\sqrt{3}h^2}\begin{bmatrix} 0 & 0 & 0 \\ 0 & 1 & 1 \\ 0 & 0 & 0 \end{bmatrix}, \quad L_h^{33} = \tfrac{8}{\sqrt{3}h^2}\begin{bmatrix} 0 & 0 & 0 \\ 0 & 1 & 0 \\ 0 & 0 & 0 \end{bmatrix}.$$

Then, from the assumptions and the definition of the operators on the infinite grid, the discrete solution, its current approximation and the corresponding error can be represented by formal linear combinations of the so-called Fourier modes, that should be appropriately defined for this case. In standard local Fourier analysis for node-based discretizations, the Fourier modes have the following form $\varphi_h(\boldsymbol{\theta}, \mathbf{x}) = e^{\imath \boldsymbol{\theta}\cdot\mathbf{x}/\mathbf{h}} = e^{\imath(\theta_1 x_1/h_1 + \theta_2 x_2/h_2)}$ with $\boldsymbol{\theta} = (\theta_1, \theta_2) \in \boldsymbol{\Theta}_h = [-\pi, \pi)^2$, and $\mathbf{x}$ being a grid-point, and they turn out to be eigenvectors of grid operators that can be represented by a single stencil, see [5, 19]. However, in our case we have to define suitable "Fourier modes" for the particular problem of edge-based discretizations. We define the following grid-functions:

$$\phi_h(\boldsymbol{\theta}, \mathbf{x}) = \alpha^1 \phi_h^1(\boldsymbol{\theta}, \mathbf{x}) + \alpha^2 \phi_h^2(\boldsymbol{\theta}, \mathbf{x}) + \alpha^3 \phi_h^3(\boldsymbol{\theta}, \mathbf{x}), \quad \mathbf{x} \in G_h, \quad \alpha^1, \alpha^2, \alpha^3 \in \mathbb{C}, \quad (2.4)$$

where

$$\phi_h^1(\boldsymbol{\theta},\mathbf{x}) = \varphi_h(\boldsymbol{\theta},\mathbf{x})\chi_{G_h^1}(\mathbf{x}), \quad \phi_h^2(\boldsymbol{\theta},\mathbf{x}) = \varphi_h(\boldsymbol{\theta},\mathbf{x})\chi_{G_h^2}(\mathbf{x}),$$
$$\phi_h^3(\boldsymbol{\theta},\mathbf{x}) = \varphi_h(\boldsymbol{\theta},\mathbf{x})\chi_{G_h^3}(\mathbf{x}),$$

denoting by $\chi_{G_h^j}(\mathbf{x})$ the characteristic function of G_h^j, that is, one if $\mathbf{x}$ belongs to G_h^j and zero elsewhere. In this way, grid-functions given in (2.4) will play the role of "Fourier modes" for the edge-based discretizations considered here, and then we can define the following space of grid-functions

$$\mathcal{F}(G_h) = \{\phi_h(\boldsymbol{\theta},\cdot) = \alpha^1\phi_h^1(\boldsymbol{\theta},\cdot) + \alpha^2\phi_h^2(\boldsymbol{\theta},\cdot) + \alpha^3\phi_h^3(\boldsymbol{\theta},\cdot),\ \alpha^1,\alpha^2,\alpha^3 \in \mathbb{C},\ \boldsymbol{\theta} \in \boldsymbol{\Theta}_h\}, \tag{2.5}$$

which will play the role of our "Fourier space". With these new definitions of Fourier modes and Fourier space, we can prove that any discrete operator given as in (2.3) leaves the subspace $\mathcal{F}(G_h)$ invariant. More concretely, the application of operator L_h to a grid-function $\phi_h \in \mathcal{F}(G_h)$ reads

$$\begin{aligned}(L_h\phi_h(\boldsymbol{\theta},\cdot))(\mathbf{x}_{k_1,k_2}^m) &= \sum_{l=1}^{3}\left(\alpha^l \sum_{(i,j)\in I^{ml}} s_{i,j}^{ml}\phi_h^l(\boldsymbol{\theta},\mathbf{x}_{k_1+i,k_2+j}^l)\right) \\ &= e^{\imath\boldsymbol{\theta}\cdot\mathbf{x}_{k_1,k_2}^m/\mathbf{h}}\sum_{l=1}^{3}\left(\alpha^l \sum_{(i,j)\in I^{ml}} s_{i,j}^{ml}e^{\imath(\theta_1(i+\delta_1^l-\delta_1^m)+\theta_2(j+\delta_2^l-\delta_2^m))}\right),\end{aligned} \tag{2.6}$$

where $\mathbf{x}_{k_1,k_2}^m \in G_h^m$. Then, from the previous expressions we can obtain

$$\begin{aligned}(L_h\phi_h(\boldsymbol{\theta},\cdot)) &= L_h\begin{bmatrix}\phi_h^1 & \phi_h^2 & \phi_h^3\end{bmatrix}\begin{bmatrix}\alpha^1\\ \alpha^2\\ \alpha^3\end{bmatrix} = \begin{bmatrix}\phi_h^1 & \phi_h^2 & \phi_h^3\end{bmatrix}\widetilde{L}_h(\boldsymbol{\theta})\begin{bmatrix}\alpha^1\\ \alpha^2\\ \alpha^3\end{bmatrix} \\ &= \begin{bmatrix}\phi_h^1 & \phi_h^2 & \phi_h^3\end{bmatrix}\begin{bmatrix}\beta^1\\ \beta^2\\ \beta^3\end{bmatrix},\end{aligned} \tag{2.7}$$

where

$$\widetilde{L}_h(\boldsymbol{\theta}) = \begin{bmatrix}\widetilde{L}_h^{11}(\boldsymbol{\theta}) & \widetilde{L}_h^{12}(\boldsymbol{\theta}) & \widetilde{L}_h^{13}(\boldsymbol{\theta})\\ \widetilde{L}_h^{21}(\boldsymbol{\theta}) & \widetilde{L}_h^{22}(\boldsymbol{\theta}) & \widetilde{L}_h^{23}(\boldsymbol{\theta})\\ \widetilde{L}_h^{31}(\boldsymbol{\theta}) & \widetilde{L}_h^{32}(\boldsymbol{\theta}) & \widetilde{L}_h^{33}(\boldsymbol{\theta})\end{bmatrix},$$
$$\text{with} \quad \widetilde{L}_h^{ml}(\boldsymbol{\theta}) = \sum_{(i,j)\in I^{ml}} s_{i,j}^{ml}e^{\imath(\theta_1(i+\delta_1^l-\delta_1^m)+\theta_2(j+\delta_2^l-\delta_2^m))}, \tag{2.8}$$

is the representation of L_h in $\mathcal{F}(G_h)$. Therefore, from expression (2.7) we can conclude that the invariance property is fulfilled. In the particular case of the discrete operator

given in Fig. 3, we easily obtain the Fourier representation, $\widetilde{L}_h(\boldsymbol{\theta})$. For instance, to compute $\widetilde{L}_h^{12}(\boldsymbol{\theta})$, one needs to consider the stencil form of the discrete operator

$$L_h^{12} = \frac{4}{\sqrt{3}h^2}\begin{bmatrix} 0 & 0 & 0 \\ 0 & 0 & 1 \\ 0 & 1 & 0 \end{bmatrix}.$$

From this latter, we can derive that $I^{12} = \{(1,0),(0,-1)\}$, and by taking into account values of (δ_1^j, δ_2^j) in (2.2), one can write out the following,

$$\begin{aligned}\widetilde{L}_h^{12}(\boldsymbol{\theta}) &= \sum_{(i,j)\in I^{12}} s_{i,j}^{12} e^{\imath(\theta_1(i+\delta_1^2-\delta_1^1)+\theta_2(j+\delta_2^2-\delta_2^1))} \\ &= s_{1,0}^{12} e^{\imath(\theta_1/2+\theta_2/2)} + s_{0,-1}^{12} e^{\imath(-\theta_1/2-\theta_2/2)} \\ &= \frac{4}{\sqrt{3}h^2}\left(e^{\imath\left(\frac{\theta_1+\theta_2}{2}\right)} + e^{-\imath\left(\frac{\theta_1+\theta_2}{2}\right)}\right) = \frac{8}{\sqrt{3}h^2}\cos\left(\frac{\theta_1+\theta_2}{2}\right).\end{aligned}$$

Finally, by computing the rest of the symbols $\widetilde{L}_h^{ml}(\boldsymbol{\theta})$ appearing in (2.8), the Fourier domain representation of the discrete operator reads

$$\widetilde{L}_h(\boldsymbol{\theta}) = \frac{8}{\sqrt{3}h^2}\begin{bmatrix} 1 & \cos\left(\frac{\theta_1+\theta_2}{2}\right) & -\cos\frac{\theta_2}{2} \\ \cos\left(\frac{\theta_1+\theta_2}{2}\right) & 1 & -\cos\frac{\theta_1}{2} \\ -\cos\frac{\theta_2}{2} & -\cos\frac{\theta_1}{2} & 1 \end{bmatrix}. \tag{2.9}$$

In the same way, many smoothing procedures have also the property that $\mathcal{F}(G_h)$ remains invariant under the action of the smoothing operator. In particular, those that are based on a splitting of the discrete operator L_h as $L_h = L_h^+ + L_h^-$, fulfill this property. This latter is a decomposition of L_h on the positive and negative parts of the operator, which correspond to the updated and non-updated unknowns before the current step, see [15]. From this decomposition, we define the relaxation operator as $S_h = -(L_h^+)^{-1}\, L_h^-$, and since each of the operators in the splitting is given as in (2.3), they satisfy the invariance property, and therefore S_h as well. For example, if we consider a decoupled Gauss-Seidel smoother in which first grid-points in G_h^1 are relaxed, after that, those in G_h^2 and finally those in G_h^3, we can write the splitting of the discrete operator in (2.9) as follows,

$$\widetilde{L}_h^+(\boldsymbol{\theta}) = \frac{8}{\sqrt{3}h^2}\begin{bmatrix} 1 & 0 & 0 \\ \cos\left(\frac{\theta_1+\theta_2}{2}\right) & 1 & 0 \\ -\cos\frac{\theta_2}{2} & -\cos\frac{\theta_1}{2} & 1 \end{bmatrix}, \quad \widetilde{L}_h^-(\boldsymbol{\theta}) = \widetilde{L}_h(\boldsymbol{\theta}) - \widetilde{L}_h^+(\boldsymbol{\theta}). \tag{2.10}$$

From this invariance property of the smoother, one can perform a local Fourier smoothing analysis by considering the corresponding Fourier domain representation of the smoothing operator on the high frequencies, that is, on the subset $\boldsymbol{\Theta}_h \backslash (-\pi/2, \pi/2]^2$, when standard coarsening is considered.

However, in order to investigate the interplay between relaxation and coarse-grid correction, which is crucial for an efficient multigrid method, it is necessary to perform a two-grid analysis which takes into account the effect of transfer operators. For this purpose, one needs to consider the error propagation operator from the two-grid method, that is,

$$M_h^{2h} = S_h^{\nu_2}(I_h - I_{2h}^h L_{2h}^{-1} I_h^{2h} L_h) S_h^{\nu_1},$$

where S_h is the smoothing procedure and the coarse-grid correction operator is composed of the discrete operators on the fine and coarse grids, L_h and L_{2h}, respectively, and the inter-grid transfer operators: restriction, I_h^{2h} and prolongation I_{2h}^h. The two-grid analysis is the basis for the classical asymptotic multigrid convergence estimates, and the spectral radius $\rho(M_h^{2h})$ of the operator M_h^{2h} indicates the asymptotic convergence factor of the two-grid method. To estimate this value, the crucial observation is that the coarse-grid correction operator, as well as the smoother, leave the so-called spaces of $2h$-harmonics, $\mathcal{F}^4(\boldsymbol{\theta}^{00})$, invariant. These subspaces are given by

$$\mathcal{F}^4(\boldsymbol{\theta}^{00}) = span\{\phi_h(\boldsymbol{\theta}^{\alpha_1\alpha_2}, \mathbf{x}) | \alpha_1, \alpha_2 \in \{0,1\}\}, \quad \text{with} \quad \boldsymbol{\theta}^{00} \in (-\pi/2, \pi/2]^2,$$

and where $\boldsymbol{\theta}^{\alpha_1\alpha_2} = \boldsymbol{\theta}^{00} - (\alpha_1 \text{sign}(\theta_1^{00})\pi, \alpha_2 \text{sign}(\theta_2^{00})\pi)$. For this reason, M_h^{2h} is equivalent to a block-diagonal matrix consisting of 12×12-blocks denoted by $\widetilde{M}_h^{2h}(\boldsymbol{\theta}^{00}) = M_h^{2h}|_{\mathcal{F}^4(\boldsymbol{\theta}^{00})}$, that is its Fourier domain representation. In this way, one can determine the spectral radius $\rho(M_h^{2h})$ by calculating the spectral radii of (12×12)-matrices, that is:

$$\rho(M_h^{2h}) = \sup_{\boldsymbol{\theta}^{00} \in (-\pi/2, \pi/2]^2} \rho(\widetilde{M}_h^{2h}(\boldsymbol{\theta}^{00})). \tag{2.11}$$

3. Mimetic finite difference schemes on triangular grids

We consider mimetic finite differences on triangular grids. This discretization is based on the discrete analogues of the differential operators gradient, divergence and rotor, satisfying discrete analogues of theorems of vector analysis. A remarkable advantage of these schemes is that we do not have to define a concrete coordinate system, which is especially interesting for considering non-structured grids. The stability and convergence of these methods is for example analyzed in [16], whose notation we follow and which we summarize next.

We start with an acute Delaunay triangulation which consists of N_D nodes, $x_i^D, i = 1, 2, \cdots, N_D$ see Fig. 4 (a), and we consider its associated dual mesh, known as Voronoi grid, see Fig. 4 (b). This mesh consists of convex polygons, each one composed of the points which are the centers of the circumscribed circles on each triangle, and that we denote as $x_k^V, k = 1, 2, \cdots, N_V$.

For a given Delaunay grid point x_i^D, we can define its associated Voronoi polygon, which contains the points that are closer to this node than to all the other Delaunay grid-points,

$$V_i = \{\mathbf{x} \in \Omega \,|\, |\mathbf{x} - \mathbf{x}_i^D| < |\mathbf{x} - \mathbf{x}_j^D|,\ j = 1, \cdots, N_D,\ j \neq i\}, \tag{3.1}$$

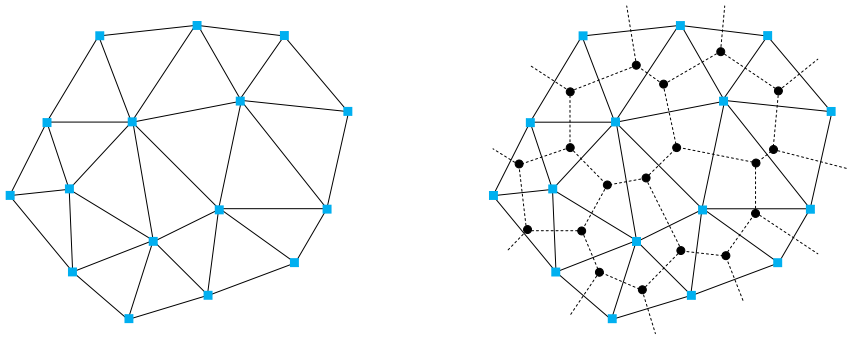

(a) (b)

Figure 4: (a) Initial Delaunay grid; and (b) corresponding Voronoi mesh.

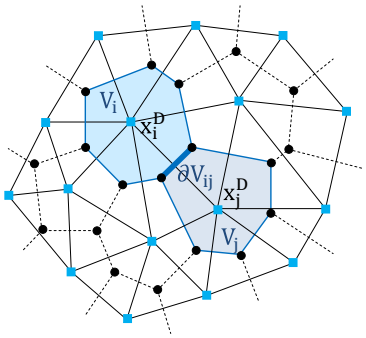

Figure 5: Voronoi polygons associated with Delaunay grid points, and corresponding notation.

and we denote by δV_{ij} the common edge of the Voronoi polygons associated with two Delaunay grid-points, if it exists, see Fig. 5.

In order to approximate the scalar functions of the continuous argument, we use scalar grid-functions that are defined on the nodes of the Delaunay grid, whose set is given by

$$H_D = \{u(\mathbf{x}) \,|\, u(\mathbf{x}) = u(\mathbf{x}_i^D) = u_i^D,\ i = 1, \cdots, N_D\}. \tag{3.2}$$

The approximation of continuous argument vector functions is however a more difficult task, and for this issue we use projections of the vectors on the directed edges. Then, we will orient the edge between two Delaunay grid-points, $\mathbf{x}_i^D$ and $\mathbf{x}_j^D$, by considering the unit vector, $\mathbf{e}_{ij}^D$, in the direction from the node with the smallest index to the node with the largest index, that is,

$$\mathbf{e}_{ij}^D = \mathbf{e}_{ji}^D, \quad i = 1, \cdots, N_D, \quad j \in \mathcal{W}^V(i) = \{j \,|\, \partial V_{ij} \neq \emptyset,\ j = 1, \cdots, N_D\},$$

see Fig. 6 (a). In this way, we define $\mathbf{H}_D$ as the set of vector grid functions $\mathbf{u}(\mathbf{x})$ on the Delaunay grid which are given by their components

$$u_{ij}^D = \mathbf{u} \cdot \mathbf{e}_{ij}^D, \quad i = 1, \cdots, N_D, \quad j \in \mathcal{W}^V(i),$$

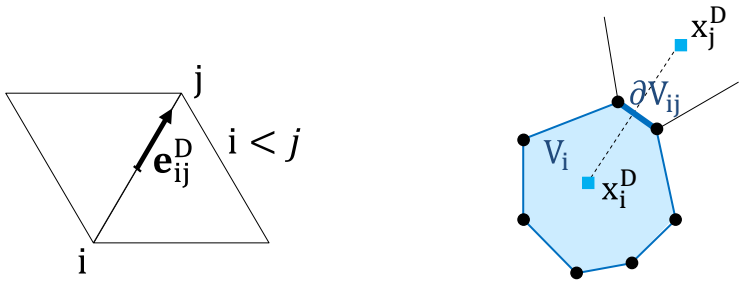

(a) (b)

Figure 6: (a) Orientation of the edge between two Delaunay grid-points, and (b) notation for the description of the divergence operator.

defined in the middle of the edges of the triangulation $\mathbf{x}_{ij}^D = \frac{1}{2}(\mathbf{x}_i^D + \mathbf{x}_j^D)$.

Once we have introduced the corresponding sets of grid functions, we can define the discrete gradient operator from the scalar grid functions to the representations of the vector grid functions, $\mathbf{grad}_h : H_D \to \mathbf{H}_D$, in the following way,

$$(\mathbf{grad}_h\, u)_{ij}^D := (\mathbf{grad}_h\, u)(\mathbf{x}_{ij}^D) \cdot \mathbf{e}_{ij}^D = \eta(i,j)\frac{u_j^D - u_i^D}{l_{ij}^D},$$

$$\text{with} \quad \eta(i,j) = \begin{cases} 1, & \text{if } j > i, \\ -1, & \text{if } j < i, \end{cases} \tag{3.3}$$

where l_{ij} is the length of the edge between nodes $\mathbf{x}_i^D$ and $\mathbf{x}_j^D$, and $\eta(i,j)$ is one or minus one depending on the direction assigned to that edge. Now, to construct the discrete operator divergence, we start from the divergence theorem on any Voronoi polyhedron V_i,

$$\int_{V_i} \text{div}\mathbf{u}\, d\mathbf{x} = \sum_{j \in \mathcal{W}^V(i)} \int_{\partial V_{ij}} (\mathbf{u} \cdot \mathbf{n}_{ij}^V)\, d\mathbf{x},$$

where n_{ij}^V is the outwards normal vector to the Voronoi edge ∂V_{ij}. By using some formulae of integration for the left- and right-hand sides, we get the expression of the discrete operator div_h from the set of vector grid functions to the set of scalar grid functions on the Delaunay grid, $div_h : \mathbf{H}_D \to H_D$, resulting as follows

$$(div_h\, \mathbf{u})_i^D = \frac{1}{\text{meas}(V_i)} \sum_{j \in \mathcal{W}^V(i)} (u_{ij}^D\, \mathbf{e}_{ij}^D) \cdot \mathbf{n}_{ij}^V\, \text{meas}(\partial V_{ij}). \tag{3.4}$$

Here meas(V_i) is the area of the Voronoi Polygon V_i around the Delaunay node x_i^D, the sum appearing in the formula goes over all the neighboring points to x_i^D, and meas(∂V_{ij}) is the length of the common edges of the corresponding Voronoi polygons, see Fig. 6 (b).

In the two dimensional case, there are two different continuous rotor operators:

$$rot\,\mathbf{u} = -\frac{\partial u_1}{\partial y} + \frac{\partial u_2}{\partial x}, \quad \text{with} \quad \mathbf{u} = (u_1, u_2), \quad \text{and} \quad \mathbf{curl}\,u = \left(\frac{\partial u}{\partial y}, -\frac{\partial u}{\partial x}\right).$$

In order to describe the discrete rotor operators, we introduce the set of scalar grid functions defined on the Voronoi grid, which are given by

$$H_V = \{u(\mathbf{x}) \,|\, u(\mathbf{x}) = u(\mathbf{x}_k^V) = u_k^V,\ k = 1, \cdots, N_V\}. \tag{3.5}$$

By using the Stokes theorem

$$\int_S (\mathrm{rot}\mathbf{u} \cdot \mathbf{n})\,\mathrm{d}\mathbf{x} = \oint_{\partial S} (\mathbf{u} \cdot \mathbf{l})\,\mathrm{d}\tau,$$

the corresponding discrete rotor operators can be defined, one from vector grid functions to scalar grid functions, $\mathrm{rot}_h : \mathbf{H}_D \to H_V$, and another on the opposite direction, that is, $\mathbf{curl}_h : H_V \to \mathbf{H}_D$. The scalar rotor operator is defined on the Voronoi grid-points and it is given by

$$(rot_h\,\mathbf{u})_k^V = \frac{\eta(i,j)\,u_{ij}^D\,l_{ij}^D + \eta(j,l)\,u_{jl}^D\,l_{jl}^D + \eta(l,i)\,u_{li}^D\,l_{li}^D}{\mathrm{meas}(D_k)}, \tag{3.6}$$

where $\mathrm{meas}(D_k)$ is the area of the triangle with vertices $\mathbf{x}_i^D, \mathbf{x}_j^D, \mathbf{x}_l^D$, associated with the Voronoi point $\mathbf{x}_k^V$, l_{ij}, l_{jl} and l_{li} are the lengths of its edges, and η is the previously defined function which is one or minus one, depending on the direction of the edges, see Fig. 7 (a). The vector rotor operator however is defined on the midpoints of the edges and is given by this difference quotient,

$$(\mathbf{curl}_h\,u)_{ij}^D = \eta(k,m)\frac{u_k^V - u_m^V}{l_{km}^V}, \tag{3.7}$$

where l_{km}^V is the distance between both Voronoi grid points $\mathbf{x}_k^V$ and $\mathbf{x}_m^V$. Notice that $l_{km}^V = \mathrm{meas}(\partial V_{ij})$, see Fig. 7 (b). All these operators that we have just introduced are consistent with the most important properties of the vector operators. In particular, doing some computations we can prove that the defined discrete operators fulfill the following properties:

$$\mathrm{rot}_h\,\mathbf{grad}_h = 0, \quad \mathrm{div}_h\,\mathbf{curl}_h = 0. \tag{3.8}$$

Since we are interested in validating the presented local Fourier analysis, we define such discrete operators on a structured triangular grid. When such a type of grid is considered, it is usual to work in stencil notation, taking advantage of the structured ordering of the unknowns appearing in the equation on each grid-point. With this purpose it is necessary to introduce a suitable numbering of the grid-points. Here, this is done by using a double index numeration, according to the unitary basis of $\mathbb{R}^2$ introduced in Section 2. It is chosen in the directions of two of the edges of the

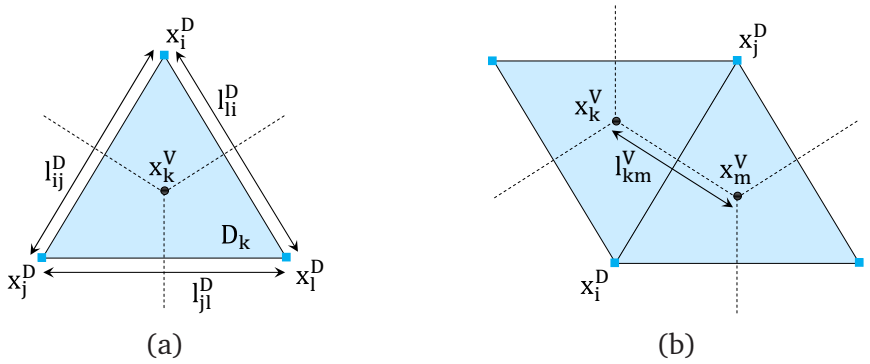

Figure 7: Notation for the definition of the (a) scalar rotor operator and the (b) vector rotor operator.

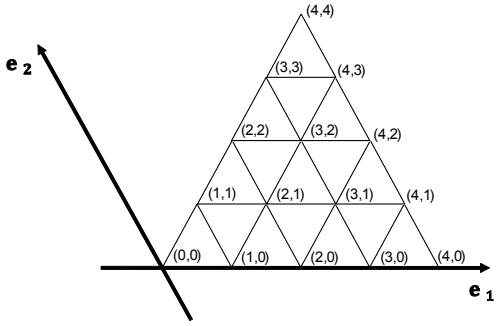

Figure 8: New basis in $\mathbb{R}^2$ fitting the geometry of a triangular domain, and local numbering for the regular grid obtained after two refinement levels.

considered triangle, as we can see in Fig. 8, where the grid obtained after applying $\ell = 2$ iterations of regular refinement (which is done by dividing each triangle into four congruent ones, connecting the midpoints of the edges), is also depicted. In this way, we have fixed the numbering for the grid-points in which scalar grid functions are defined. However, as previously commented, for vector grid functions we consider the projections on the midpoints of the edges, so we also need a numbering for such points. To do that, we differentiate between the components on each "type of edge", as we can see in Fig. 2 (b). Then, we assign the same index to four different points, one vertex and the three midpoints of these associated edges.

A structured triangular grid can be characterized by two angles α and β. Since all the parameters (areas, distances, etc.) involved in the expressions of the discrete operators can be easily written as a function of the angles α and β, after simple computations we can obtain the stencils of gradient, divergence and rotor operators in terms of these geometric parameters, as we can see in Fig. 9. Notice that $\mathbf{grad}_h$ and $\mathbf{curl}_h$ operators are defined on the midpoints of the edges, and in the figure we only display such stencils corresponding to a grid-point located at the midpoint of a horizontal edge. However, the corresponding stencils for the other two types of grid-points can be anal-

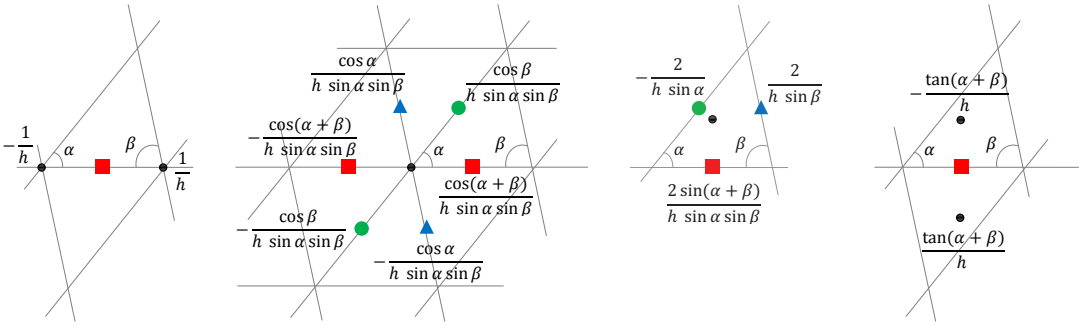

Figure 9: Stencils for the discrete (a) $\mathbf{grad}_h$, (b) div_h, (c) rot_h and (d) $\mathbf{curl}_h$ operators on a general triangular grid characterized by angles α and β.

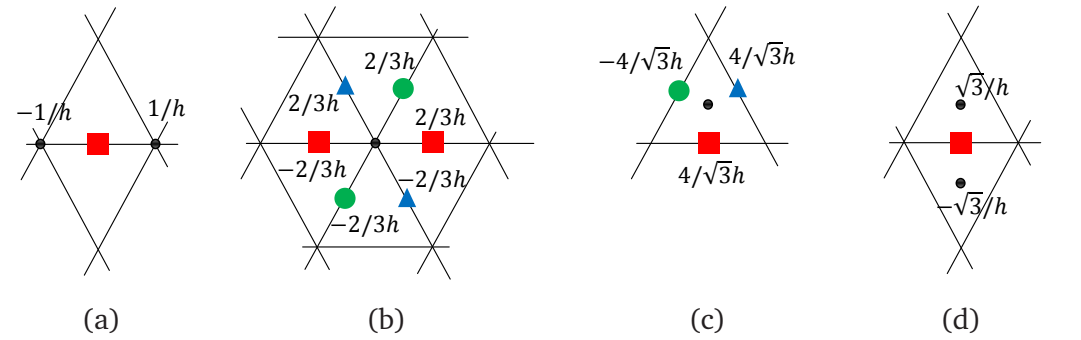

Figure 10: Stencils for the discrete (a) $\mathbf{grad}_h$, (b) div_h, (c) rot_h and (d) $\mathbf{curl}_h$ operators on equilateral triangular grids.

ogously computed. As an example, the stencils corresponding to the discrete gradient, divergence and rotor operators on an equilateral triangular grid are shown in Fig. 10. The obtained stencils can be combined to discretize more complex operators.

4. Local Fourier analysis results

To illustrate the performance of the previously described local Fourier analysis, we use the vector Laplace operator as model problem,

$$-\mathbf{grad}\,\mathrm{div}\,\mathbf{u} + \mathbf{curl}\,\mathrm{rot}\,\mathbf{u} = \mathbf{f}, \quad \text{in } \Omega. \tag{4.1}$$

Considering the discrete operators previously introduced, we can obtain the stencils corresponding to our problem on a structured triangular grid characterized by angles α and β. The stencils corresponding to the discretization of the $-\mathbf{grad}\,\mathrm{div}$ operator on

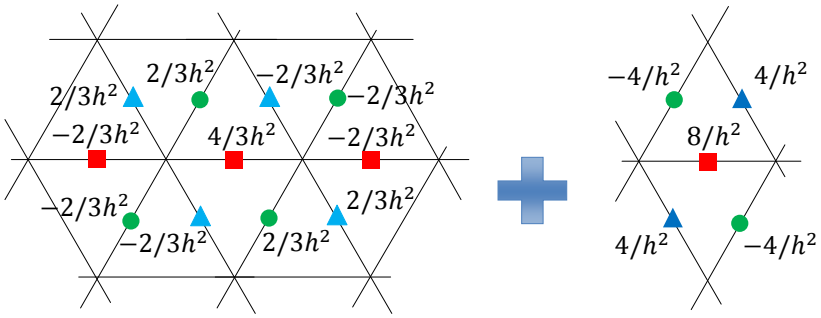

Figure 11: Stencils composing the discretization of the vector Laplace operator on equilateral triangular grids.

a grid-point located at the horizontal edges are given by

$$L_{1,h}^{11} = \frac{1-\cot\alpha\cot\beta}{h^2}\begin{bmatrix} 0 & 0 & 0 \\ -1 & 2 & -1 \\ 0 & 0 & 0 \end{bmatrix},$$

$$L_{1,h}^{12} = \frac{\cot\alpha}{h^2\sin\beta}\begin{bmatrix} 0 & 0 & 0 \\ 0 & 1 & -1 \\ 0 & -1 & 1 \end{bmatrix}, \quad L_{1,h}^{13} = \frac{\cot\beta}{h^2\sin\alpha}\begin{bmatrix} 0 & 0 & 0 \\ 0 & 1 & -1 \\ -1 & 1 & 0 \end{bmatrix}.$$

Regarding the operator $\mathbf{curl}\,\mathrm{rot}$, the obtained stencils are:

$$L_{2,h}^{11} = \frac{-4(\cot\alpha+\cot\beta)}{h^2\cot(\alpha+\beta)}\begin{bmatrix} 0 & 0 & 0 \\ 0 & 1 & 0 \\ 0 & 0 & 0 \end{bmatrix},$$

$$L_{2,h}^{12} = \frac{2}{h^2\sin\beta\cot(\alpha+\beta)}\begin{bmatrix} 0 & 0 & 0 \\ 0 & 0 & -1 \\ 0 & -1 & 0 \end{bmatrix}, \quad L_{2,h}^{13} = \frac{2}{h^2\sin\alpha\cot(\alpha+\beta)}\begin{bmatrix} 0 & 0 & 0 \\ 0 & 1 & 0 \\ 0 & 1 & 0 \end{bmatrix}.$$

As an example, the stencils corresponding to an equilateral triangle are shown in Fig. 11. Note that we only present the corresponding stencils for the vector component located at the midpoints of the "horizontal" edges. However, the expressions for the other two components can be similarly obtained.

Our aim is to find an efficient multigrid method for this vector problem. A geometric multigrid method is going to be applied, so we need to define the hierarchy of grids necessary to perform the algorithm. To this purpose, we apply regular refinement to an initial triangular domain, obtaining a regular structured triangular grid, and we consider the midpoints of the edges as the grid-points where the unknowns will be located, see Fig. 12. Notice that we have a hierarchy of non nested grids.

Once we have established the hierarchy of grids, we have to find appropriate components for the multigrid algorithm. To this purpose, we use the local Fourier analysis

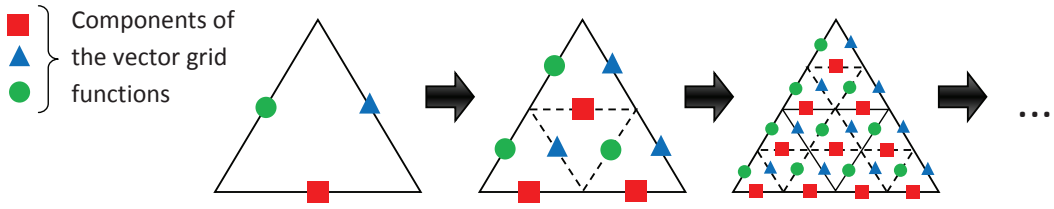

Figure 12: Hierarchy of grids to perform the geometric multigrid method, and location of the unknowns.

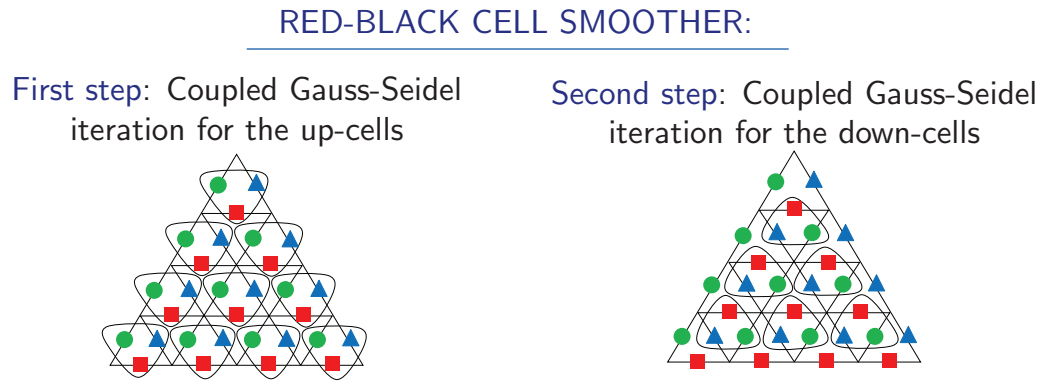

Figure 13: Two relaxation steps composing the red-black cell smoother.

presented in Section 2. Regarding the inter-grid transfer operators, weighted averages of the nearest neighbors are considered to define the restriction and the interpolation methods. We focus on the choice of the smoother, since it is usually the component of the algorithm which has more influence on the performance of the geometric multigrid method. We have designed the called here red-black cell smoother. This relaxation process consists of two partial steps, as seen in Fig. 13. In the first one we visit each up-oriented triangle and we simultaneously relax the three components located at its edges. And in the second step, we go over all the down-oriented triangles, and the corresponding three components are updated together. The combination of these two steps gives rise to a very efficient smoother for the problem considered, as we will see. Notice that small 3×3 systems must be solved in the relaxation process.

In order to show the good behavior of this smoother, we present some results obtained by the local Fourier analysis introduced in Section 2. First, we consider a structured equilateral triangular grid, and in Table 1 we compare the behavior of the multigrid based on the red-black cell relaxation with that based on a decoupled symmetric Gauss-Seidel smoother. In this latter, first the components associated with the horizontal edges are relaxed, after that, those corresponding to the edges in the direction of the second axis in the system of coordinates, and finally the third type of components are updated. Notice that a decoupled symmetric Gauss-Seidel is used in order to have a fair comparison regarding the amount of work per iteration step, since in this way,

Table 1: LFA two-grid convergence factors, ρ, and measured W-cycle asymptotic convergence rates, ρ_h for an equilateral triangle, comparing the behavior of the multigrid algorithm using the red-black cell smoother and a decoupled symmetric Gauss-Seidel smoother.

	Red-Black cell		Decoupled Symmetric GS	
ν	ρ	ρ_h	ρ	ρ_h
1	0.260	0.262	0.448	0.443
2	0.196	0.192	0.281	0.276
3	0.118	0.115	0.213	0.210
4	0.101	0.098	0.171	0.171

both smoothers update twice each unknown. Then, for different numbers of smoothing steps, the two-grid convergence factors predicted by local Fourier analysis, ρ, are shown together with the asymptotic convergence factors experimentally computed by using a W-cycle, ρ_h. First of all, we observe that the LFA predicts very accurately the convergence rates obtained in all the cases. Moreover, we see that this new smoother improves the results obtained with the decoupled Gauss-Seidel smoother.

However, the highly satisfactory factors obtained with the red-black cell smoother for equilateral triangles deteriorate as the triangular grid becomes anisotropic. This behavior can be seen in Fig. 14, where for a wide range of triangulations characterized by two of their angles, the two-grid convergence factor predicted by LFA is displayed. From this figure, it is clear that the red-black cell smoother is not robust with respect to the geometry of the grid, and then, the convergence becomes significantly worse when one of the angles characterizing the triangular grid is very small.

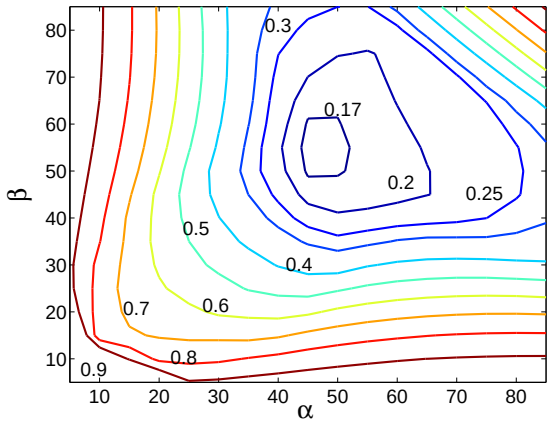

Figure 14: Spectral radius ρ predicted by LFA for different triangular grids as a function of two of their angles, using the red-black cell smoother.

Therefore, when an anisotropic grid is considered, a stronger smoother is needed in order to obtain an efficient multigrid algorithm. It is well-known that for node-based discretizations on triangular grids, line-wise relaxation procedures are preferred over

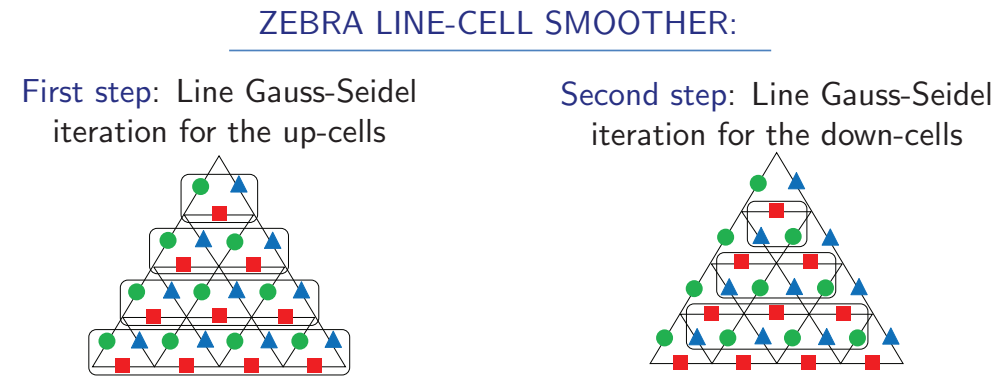

Figure 15: Two relaxation steps composing the zebra line-cell smoother.

point-wise smoothers to deal with such meshes characterized by a small angle, see [14]. Then, our purpose here is to extend the idea of the red-black cell smoother to a line-wise procedure. This is done by combining again two separate partial steps, which are schematized in Fig. 15. In the first one we visit each row of up-oriented triangles and we simultaneously relax the unknowns located at the edges of all these triangles. Then, the second partial step consists of simultaneously updating the unknowns located in the rows of down-oriented triangles. Both steps are done in the direction from the edge to the vertex of the triangular domain, and in a Gauss-Seidel manner. In this way, we will see that combining both partial steps, we obtain a very strong smoother, capable to deal with the problematic anisotropic grids. Notice that for the relaxation of a row of unknowns, a block-tridiagonal system has to be solved.

To demonstrate the suitability of the zebra line-cell relaxation to deal with anisotropic triangular meshes, we have performed a local Fourier analysis for this kind of smoother. Notice that the extension of the analysis to this type of line smoothers is standard since in this case, each partial step composing the whole iteration can be written in terms of a splitting of the discrete operator, as commented in Section 2. This analysis turns out very useful to know exactly when this type of block-smoother has to be used instead of the cheaper red-black cell relaxation. To illustrate this situation, we will use a representative triangular grid giving rise to this type of anisotropies obtained when one of the angles characterizing the triangular grid is very small. For example, an isosceles triangular grid with common angle $\alpha = \beta = 80^{\mathrm{o}}$ is considered. In Table 2, both relaxations proposed in this work are considered: the red-black cell and the zebra line-cell smoothers. The two-grid convergence factors predicted by LFA are compared with those experimentally computed by using a W-cycle for different numbers of smoothing steps, and it is clearly seen the good correspondence between the theoretical and the computational results. Moreover, as we can observe, while the red-black cell smoother is not capable to handle the effects of the anisotropic grid, the zebra line-cell smoother provides very good convergence factors. Then, we can conclude that the proposed zebra line-cell smoother is strong enough to deal with anisotropic triangular grids.

Table 2: LFA two-grid convergence factors, ρ, and measured W-cycle asymptotic convergence rates, ρ_h for an isosceles triangular grid with common angle $\alpha = \beta = 80^{\circ}$, comparing the behavior of the multigrid algorithm using the red-black cell smoother and a the zebra line-cell smoother.

	Red-Black cell		Zebra line-cell	
ν	ρ	ρ_h	ρ	ρ_h
1	0.834	0.823	0.246	0.242
2	0.696	0.685	0.196	0.185
3	0.580	0.570	0.097	0.091
4	0.484	0.470	0.089	0.085

5. Conclusions and future work

In this work, we have introduced a local Fourier analysis technique for edge-based discretizations on triangular grids. To perform this analysis we had to take into account that for the considered discretizations the stencil corresponding to the discrete operator is not the same for the grid-points located at edges of different orientation, which makes the analysis special. This technique is developed for two-dimensional problems and for discretizations that have only one unknown per edge. However, it can be easily extended to three-dimensional problems and to discretizations with several unknowns per edge, as for example high-order discretizations. The presented local Fourier analysis tool has been validated by using the mimetic finite difference discretization of the vector Laplace problem, and the results presented show that the analysis gives very accurate predictions of the convergence of the multigrid method. For this model problem, also appropriate smoothers have been designed to its efficient solution on different grid geometries. This latter could be valuable for the solution of the problem on more complex computational domains, by the design of a block-wise multigrid algorithm on semi-structured grids, that can adjust easily relative complex geometries. Regarding other future research lines, the local Fourier analysis presented in this paper will be the basis for the design of special smoothers for more complicated vector problems in the future.

Acknowledgments This work was supported by the Spanish project FEDER/MCYT MTM2010-16917 and the DGA (Grupo consolidado PDIE).

References

[1] D.N. ARNOLD, R.S. FALK AND R. WINTHER, *Preconditioning in H(div) and applications,* Math. Comp., 66 (1997), pp. 957-984.
[2] R. BECK, *Algebraic multigrid by components splitting for edge elements on simplicial triangulations,* Preprint SC 99-40, ZIB, Dec. 1999.
[3] A. BORZÌ, *High-order discretization and multigrid solution of elliptic nonlinear constrained optimal control problems,* J. Comput. Appl. Math., 200 (2007), pp. 67–85.
[4] A. BOSSAVIT, *Computational Electromagnetism,* Academic Press, San Diego, 1998.

[5] A. Brandt, *Multi-level adaptive solutions to boundary-value problems*, Math. Comput., 31 (1977), pp. 333–390.
[6] A. Brandt, *Rigourous quantitative analysis of multigrid I. Constant coefficients two level cycle with L2 norm,* SIAM J. Numer. Anal., 31 (1994), pp. 1695–1730.
[7] F.J. Gaspar, J.L. Gracia, F.J. Lisbona, *Fourier Analysis for multigrid methods on triangular grids,* SIAM J. Sci. Comput., 31 (2009), pp. 2081–2102.
[8] P.W. Hemker, W. Hoffmann and M.H. van Raalte, *Fourier two-level analysis for discontinuous Galerkin discretization with linear elements,* Numer. Linear Alg. Appl., 11 (2004), pp. 473–491.
[9] W. Hackbusch, *Multi-grid methods and applications,* Springer, Berlin, 1985.
[10] R. Hiptmair and J. Xu, *Nodal auxiliary space preconditioning in H(curl) and H(div) spaces,* SIAM Journal Numerical Analysis, 45 (2007), pp. 2483–2509.
[11] J.J. Hu, R.S. Tuminaro, P.B. Bochev, C.J. Garasi, and A.C. Robinson, *Towards and h-independent algebraic multigrid method for Maxwell's equations,* SIAM Journal on Scientific Computing, 27 (2006), pp. 1669–1688.
[12] K. Lipnikov, G. Manzini, M. Shashkov, *Mimetic finite difference methods,* Journal of Computational Physics, 257 (2014), pp. 1163-1227.
[13] S. Reitzinger and J. Schöberl, *An algebraic multigrid method for finite element discretizations with edge elements,* Numer. Linear Alg. Appl., 9 (2002), pp. 223–238.
[14] C. Rodrigo, F.J. Gaspar and F.J. Lisbona, *Geometric multigrid methods on triangular grids: Application to semi-structured meshes,* Lambert Academic Publishing, Saarbrücken, 2012.
[15] U. Trottenberg, C.W. Oosterlee, A. Schüller, *Multigrid,* Academic Press, New York, 2001.
[16] P.N. Vabishchevich, *Finite-difference approximation of mathematical physics problems on irregular grids,* CMAM, 5 (2005), pp. 294–330.
[17] T. Weiland, *A discretization method for the solution of Maxwell's equations for six-component fields,* Electron. Commun. AEU 31 (1977), pp. 116-120.
[18] P. Wesseling, *An Introduction to Multigrid Methods,* John Wiley, Chichester, UK, 1992.
[19] R. Wienands, W. Joppich, *Practical Fourier analysis for multigrid methods,* Chapman and Hall/CRC Press, 2005.
[20] R. Wienands, C.W. Oosterlee and T. Washio. *Fourier analysis of GMRES(m) preconditioned by multigrid,* SIAM J. Sci. Comput., 22 (2000), pp. 582–603.